Spatially Separated Spin Carriers in Spin-Semiconducting Graphene Nanoribbons

Z. F. Wang,[1] Shuo Jin,[2] and Feng Liu[1,*]

[1]*Department of Materials Science and Engineering, University of Utah, Salt Lake City, Utah 84112, USA*
[2]*Department of Physics, Beihang University, Beijing 100191, China*

(Received 2 May 2013; published 29 August 2013)

A graphene nanoribbon with sawtooth edges has a ferromagnetic ground state. Using first-principles and tight-binding model calculations, we show that, under a transverse electrical field, the sawtooth graphene nanoribbons become a spin semiconductor whose charge carriers are not only spin polarized in energy space but also spatially separated at different edges. Low-energy excitation produces spin-up electrons localized at one edge and spin-down holes at the opposite edge, and the excitation energy of spin carries can be tuned by the electric field to reach a new state of spin gapless semiconductor. Also, the spin semiconducting states are shown to be robust against at least 10% edge disorder. These features demonstrate a good tunability of spin carriers for spintronics applications.

DOI: 10.1103/PhysRevLett.111.096803 PACS numbers: 73.22.Pr, 61.48.Gh, 75.70.Ak

A spintronic device uses spin instead of charge as an information carrier, by taking advantage of the spin polarized electronic energy state in a material. A well-known example is half-metal [1,2], in which one spin state is metallic while the other spin state has a semiconducting gap, as illustrated in Fig. 1(a), so that the carriers are 100% spin polarized with only one spin state conducting. Another interesting example is a spin semiconductor or a spin gapless semiconductor [3–7], in which both spin states have a gap but are relatively energy shifted, as illustrated in Figs. 1(b) and 1(c), so that the carriers are also 100% spin polarized with either electrons conducting one spin or holes conducting a different spin. Here, we demonstrate the realization of a spin semiconductor in graphene nanoribbons (GNRs), whose spin carries are not only polarized in energy space but also spatially separated at the two opposite edges of GNRs. This additional separation of spins in Cartesian space gives another degree of freedom in manipulating and controlling spins in spintronic devices.

Figure 1 illustrates the basic idea of our proposed spin-semiconducting GNR, in comparison with the half-metallic GNR. It is well known that a GNR with two straight zigzag edges has an antiferromagnetic (AFM) ground state. First-principles calculations predicted that, under a transverse electrical field, the zigzag GNR becomes a half-metal [2]. The half-metallicity results from the opposite energy-level shift of the AFM-coupled edge states: one pair of the same spin states from two edges closing up and the other pair separating apart, as illustrated in Fig. 1(a). Now, if the GNR has a ferromagnetic (FM) ground state, such as the one shown in Fig. 1(e) with sawtooth (ST) zigzag edges [8], then our first-principles calculations predict that, under a transverse electrical field [as marked in Fig. 1(e)], the FM ST GNR becomes a spin semiconductor, which results from the opposite energy-level shift of the FM-coupled edge states: one pair of opposite spin states from two edges closing up and the other pair separating apart, as illustrated in Figs. 1(b) and 1(c). Another interesting difference is that in the half-metallic GNR, the spins have energy selectivity but not spatial selectivity, because the electrons with the same spin are conducting at both edges, as illustrated in Fig. 1(d) (upper panel). In contrast, in the spin-semiconducting ST GNR, the spins have both energy and spatial selectivity: when the electrons of one spin conduct at one edge, the holes of the other spin must conduct at the opposite edge with a different energy, as illustrated in Fig. 1(d) (lower panel).

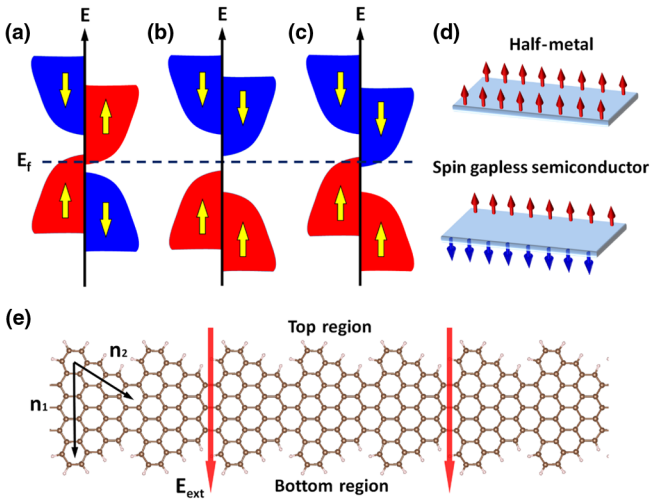

FIG. 1 (color online). Schematic band structures of (a) half-metal, (b) spin-semiconductor, and (c) spin gapless semiconductor. The up and down yellow arrows denote spin-up (red) and spin-down (blue) states, respectively. (d) Schematic spatial distribution of the spin polarized edge states for the half-metal and spin gapless semiconductor. (e) Atomic structure of an (n_1, n_2) ST GNR. (n_1, n_2) denotes the size of the ST GNR. The external electric field (E_{ext}), applied across the ST GNR pointing from top to bottom, is indicated by the downward red arrow.

To design a FM GNR, we adopt a unified geometric rule recently developed by Yu *et al.* for determining the magnetism in graphene-based nanostructures [8], which stated that two zigzag edges in graphene are FM coupled if their angles are 0° or 120° to each other, because the atoms on the two edges are on the same A or B sublattice, and AFM coupled if their angles are 60° or180°, because the atoms on the two edges belong to different sublattices. Specifically, we consider a FM ST-edged GNR, as shown in Fig. 1(e). We use two integers (n_1, n_2) to label the size of a ST GNR, which is the number of hexagonal rings along the $\vec{n}_1$ and $\vec{n}_2$ directions, as marked in Fig. 1(e).

Our first-principles calculations are carried out in the framework of the generalized gradient approximation of Perdew-Burke-Ernzerhof for the exchange-correlation functionals [9] using the VASP package [10]. All self-consistent calculations were performed with a plane-wave cutoff of 600 eV on a $21 \times 1 \times 1$ Monkhorst-Pack k-point mesh. A supercell with a vacuum layer of 10 Å is used to ensure decoupling between neighboring slabs. For structural relaxation, all the atoms are allowed to relax until atomic forces are smaller than 0.01 eV/Å. The optimized lattice constant for the (5,4) ST GNR is $L = 8.72$ Å.

First, the band structure of the (5,4) ST GNR without spin is shown in Fig. 2(a), in which two subbands cross the Fermi level. The existence of such dispersionless subbands is originated from the special sawtooth shape of the ST GNR, which also exists in zigzag-edged triangle nanohole graphene superlattices [8,11], but is absent in armchair-edged nanohole graphene superlattices [12]. Next, we turn to the spin degree of freedom. Interestingly, we found that the ground state of the ST GNR is FM with a magnetic moment of $2\mu_B$. The two edge subbands [Fig. 2(a)] split into two groups with opposite spins and a finite spin band gap opens up (E_s, between the subbands of VB2 and CB1), as schematically shown in Fig. 2(b). Here, the minimum band gap is between the subbands with different spins. Thus, we call it a spin semiconductor, as illustrated in Fig. 1(b). The number of edge subbands in a ST GNR can be easily understood from the Lieb's theorem [13] on a bipartite lattice; i.e., it is determined by the number of sublattice difference: $|n_A - n_B|$, where n_A (n_B) is the number of atoms on the A (B) sublattice of the ST GNR. For the (5,4) ST GNR, there are 38 carbon atoms in the unit cell, and among them 20 belong to the A site and 18 belong to the B site. Consequently, $|n_A - n_B| = 2$, consistent with our calculated edge subbands and magnetic moment.

Now, we turn to the focus of this work, the response of such a spin semiconductor to a transverse electric field. By applying a downward transverse electric field to the ST GNR, as shown in Fig. 1(e), the edge subbands with the same spins (VB1 and VB2, CB1 and CB2) will split away from each other with the increasing strength of the electric field, as shown in Figs. 2(c) and 2(d). Meanwhile, the spin

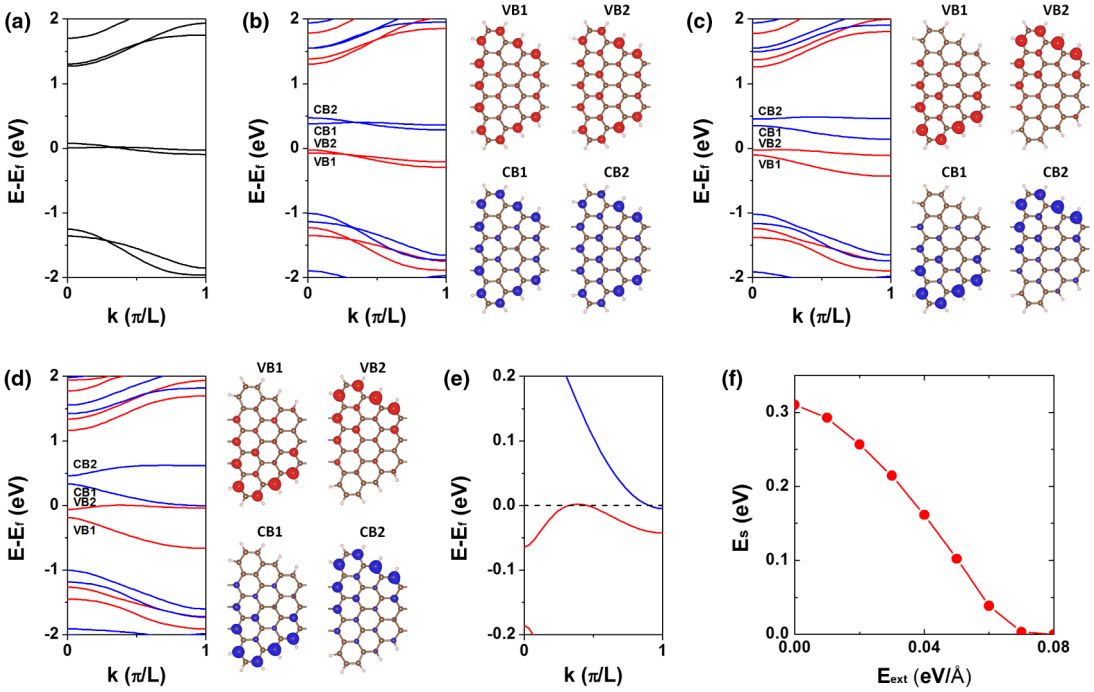

FIG. 2 (color online). (a) Band structure of (5,4) ST GNR without the spin. (b)–(d) Spin polarized band structures and partial charge density distribution of a (5,4) ST GNR with $E_{\text{ext}} = 0.0$, 0.04, and 0.08 eV/Å, respectively. The red (blue) color denotes spin-up (spin-down) states. VB1, VB2, CB1, and CB2 are the labels for the edge subbands, whose partial charge densities are plotted. (e) Zoom-in band structure of (d) around the Fermi level, in which the spin band gap is zero. (f) Spin band gap as a function of E_{ext} for a (5,4) ST GNR.

band gap will decrease in the same process [Fig. 2(f)], and eventually closes down at $E_{\text{ext}} = 0.08$ eV/Å, which can be clearly seen in Fig. 2(e). After the spin band gap closes down, the spin semiconductor becomes a spin gapless semiconductor, in which the carriers (both electrons and holes) are 100% spin polarized. If we further tune the Fermi level by a gate voltage, either electrons or holes can be used as charge carriers for transport, but with opposite spin. This spin tunable feature in a spin gapless semiconductor can be very useful to design qubits for quantum computing, data storage, and coding or decoding.

Another interesting phenomenon we found in the ST GNR is that the charge carriers are not only spin polarized in energy space, but also spatially separated at different edges under the transverse electric field, because the spatial symmetry of the spin polarized edge states is broken near the Fermi level. For $E_{\text{ext}} = 0$ [Fig. 2(b)], the charge densities of the four subbands (VB1, VB2, CB1, CB2) are uniformly distributed at the two edges for both spins. However, when the transverse electric field is turned on, the charge densities for these four subbands become localized at different sides of the ST GNR [Figs. 2(c) and 2(d)]. For the spin-up (spin-down) subbands, VB1 (CB1) is localized at the bottom region while VB2 (CB2) is localized at the top region of the ST GNR. Furthermore, such spatially separated charge densities are found to be insensitive to the strength of the transverse electric field, showing little change with the increasing electric field. Generally, it is well known that the electrons and holes can be separated in a perpendicular magnetic field or in type-II superlattices [14]. Here, our finding demonstrates a new physical mechanism to separate electrons and holes with different spins by applying a transverse electric field to the ST GNR. Experimentally, we suggest that such spin spatial separation is detectable in the spin polarized STM measurement. When a spin polarized STM tip scans over the ST GNR, if the spin orientation of the STM tip is same as that of the ST GNR edge atom, the tunneling current should increase, or decrease otherwise. Thus, under a negative (occupied states generating the current) or positive (unoccupied states generating the current) bias voltage, spin polarized electrons or holes on different edges can be directly mapped out. The efficient separation of the electrons and holes in a ST GNR makes it also potentially useful for solar cell devices, which can greatly reduce the radiative recombination and enhance the carrier collection efficiency after photoexcitation.

Lastly, we try to get a better understanding about the formation mechanism of the spin gapless semiconductor in a ST GNR. Similar to the mechanism for realizing half-metal in a zigzag GNR [2], the transverse electric field also induces an opposite energy-level shift for the spin polarized edge states in a ST-GNR; i.e., the spin polarized edge states in the top (bottom) region are shifted upwards (downwards). As shown in Figs. 3(a)–3(c), the spin

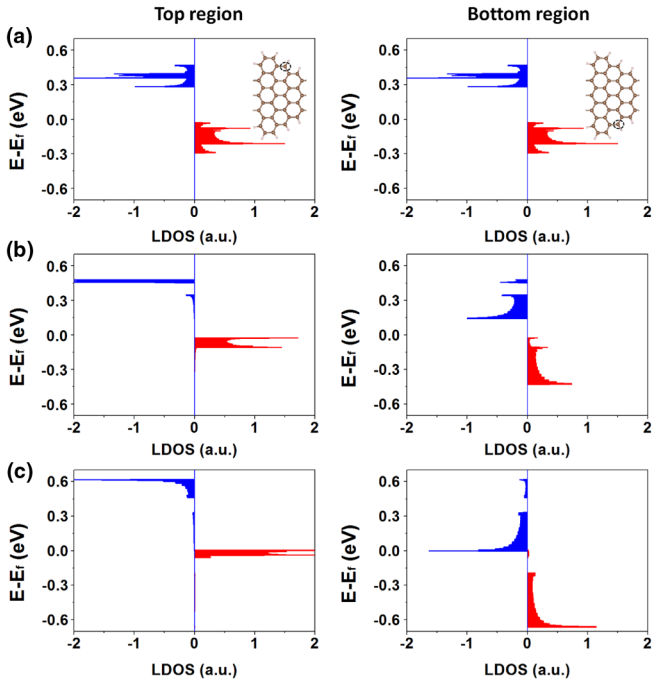

FIG. 3 (color online). Spin polarized edge LDOS for a (5,4) ST GNR under the transverse electric field. (a) $E_{\text{ext}} = 0.0$ eV/Å, (b) $E_{\text{ext}} = 0.04$ eV/Å, and (c) $E_{\text{ext}} = 0.08$ eV/Å. The spin-up (spin-down) LDOS is plotted with red (blue) color. The edge atoms of a ST GNR, at which site the LDOS are plotted, are labeled in the insets of (a). Unit a.u. means arbitrary unit.

polarized LDOS in the top (bottom) region moves upwards (downwards) with the increasing electric field, and the spin band gap closes up at $E_{\text{ext}} = 0.08$ eV/Å. In addition, under the transverse electric field, the LDOS in the top and bottom regions becomes asymmetric, and only one spin component has the dominant contribution at each edge. Therefore, it is the spatial localization of the FM edge states around the Fermi level that results in the spin gapless semiconductor in ST GNRs.

Our first-principles results can be well reproduced by a single-orbital tight-binding (TB) Hubbard model under mean-field approximation [15–18]. The TB Hamiltonian of a ST GNR is given by

$$H_0 = \gamma \sum_{\langle i,j\rangle,\sigma} c_{i\sigma}^{+} c_{j\sigma} + U \sum_{i,\sigma} [\langle n_{i,-\sigma}\rangle - 1/2] n_{i\sigma}, \quad (1)$$

where $c_{i\sigma}^{+}$, $c_{i\sigma}$, and $n_{i\sigma}$ are creation, annihilation, and number operators for an electron of spin σ in the π orbital centered on the ith carbon atom, respectively. $\gamma = -2.6$ eV is the nearest-neighbor hopping integral and $U = 2.75$ eV is the on-site Coulomb energy. The additional parameter U is necessary because of the localized states enhancing the electron-electron interactions near the saw-tooth edges. $n_{i\uparrow,\downarrow}$ is computed self-consistently from

$$\langle n_{i\sigma}\rangle = \int_{-\infty}^{E_f} g_{i\sigma}(E) dE, \quad (2)$$

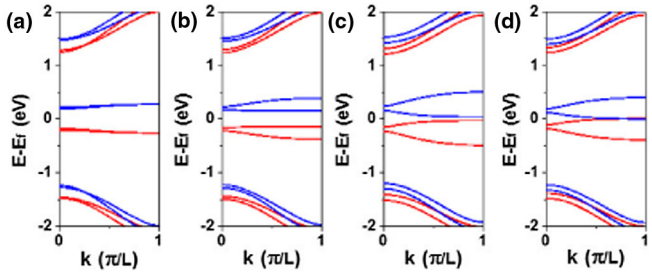

FIG. 4 (color online). (a)–(d) Spin polarized TB band structures of a (5,4) ST GNR with $E_{\text{ext}} = 0.0$, 0.03, 0.06, and 0.063 eV/Å, respectively. The red (blue) color denotes spin-up (spin-down) bands.

where $g_{i\sigma}$ is the local spin density of states obtained from Eq. (1). Fermi energy E_f is set to zero, corresponding to the undoped case. The application of the transverse electric field adds an additional term to the Hamiltonian [15]:

$$H = H_0 + \sum_{i\sigma} E_{\text{ext}}(y_i - y_m) n_{i\sigma}, \tag{3}$$

where the first term is given by Eq. (1) and the second term is the vertical potential due to the transverse electric field E_{ext}. y_i is the transverse coordinate of the ith atom in the ST GNR, and y_m is the middle coordinate of the ST GNR.

Solving Eqs. (1)–(3) self-consistently, the spin polarized TB band structures for the (5,4) ST GNR are shown in Fig. 4. We can see that there are two edge subbands for both spins and they split away from each other with the increasing electric field. When the electric field reaches 0.063 eV/Å the spin band gap closes and the ST GNR becomes a spin gapless semiconductor. The spatial distribution of these four edge subbands is also checked. Without the electric field, they are distributed uniformly at the two edges; with the electric field, they become localized at different edges. All of these features are qualitatively consistent with our first-principles results. Using this TB model, we further studied the size effect for the ST GNR under electric field. For a fixed strength of electric field, the energy-level shift of the edge states depends on the voltage drop between the two edges. Consequently, the critical electric field for closing the spin band gap is

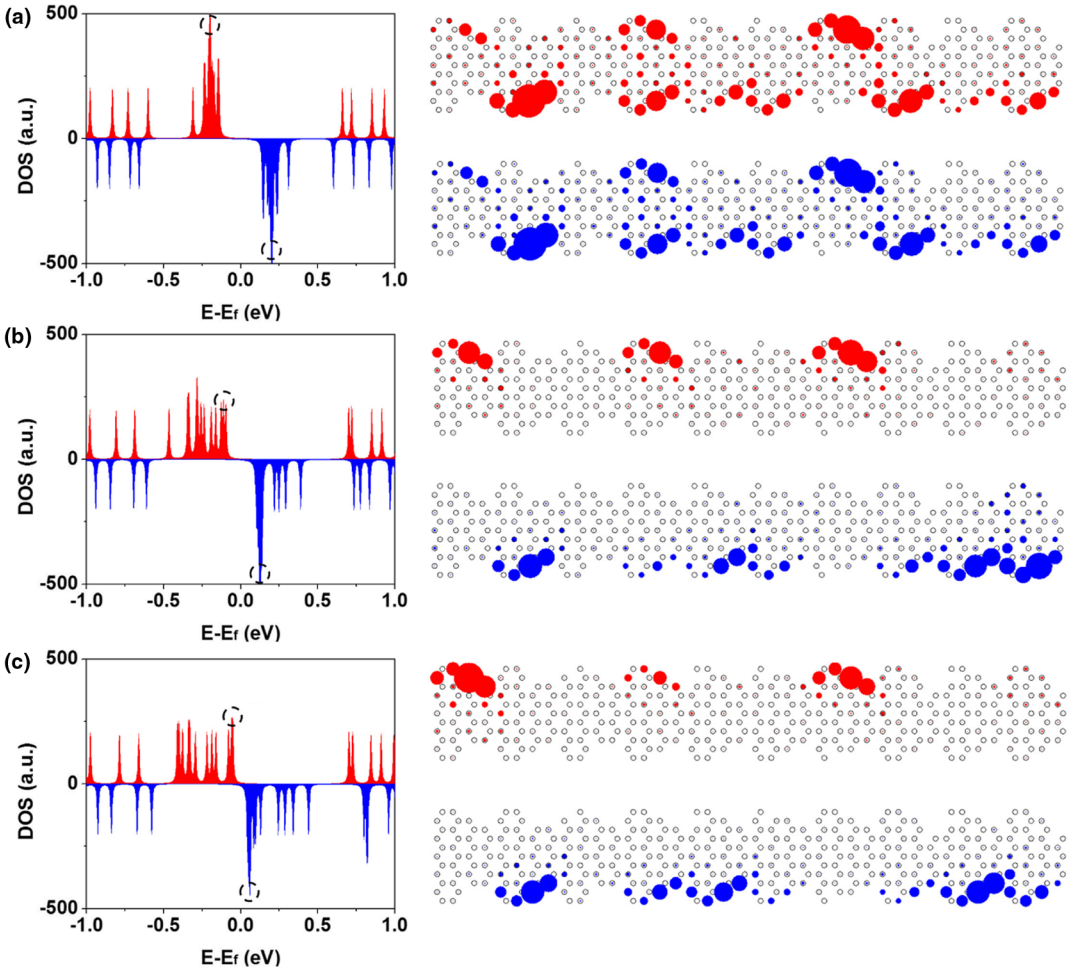

FIG. 5 (color online). (a)–(c) Left-hand panel: Spin polarized DOS of a (5,4) ST GNR with 10% edge vacancy from TB calculations for $E_{\text{ext}} = 0.0$, 0.03, and 0.06 eV/Å, respectively. Right-hand panel: Real-space distribution of LDOS for the states with the energies marked by the circle in the left-hand panel. The red (blue) color denotes spin-up (spin-down) states. Unit a.u. means arbitrary unit.

expected to decrease with the increasing width of the ST GNR. From our calculations, we found that the critical field to create the spin gapless semiconductor for the (4,4), (5,4), and (6,4) ST GNR is 0.095, 0.063, and 0.046 eV/Å, respectively. On the other hand, the nature of spatial separation of the spin carriers in a ST GNR is very robust, which does not depend on the ST GNR size.

Real samples of GNRs are likely to contain structural defects and impurities. Previous theoretical studies have shown that the magnetism in GNRs can be suppressed by a high concentration of edge defects [19,20]. Therefore, one important question is, how robust are the spatially separated spin semiconductor states against edge disorder? We have constructed a supercell made of 10 unit cells of (5,4) ST GNR, containing 10% (Fig. 5) and 20% randomly distributed edge vacancies. Using the TB model, the DOS of the defected (5,4) ST GNR under different electric fields are calculated, and the results for the 10% case are shown in Fig. 5. Mainly the vacancy makes the DOS nonuniform along the edge, but it does not change the relative distribution between the two edges. For example, without the field [Fig. 5(a)], the spin-up (below Fermi level) and spin-down (above Fermi level) edge states are symmetric about the Fermi level, and the LDOS has about equal distribution at both edges. Turning on the field, the edge states become asymmetric about the Fermi level [Figs. 5(b) and 5(c)]. The spin gap decreases with the increasing electric field, and meanwhile, the spin-up and -down edge states become localized at opposite edges. All these features are qualitatively the same with the perfect GNR results, indicating that the spin-semiconductor properties can survive up to at least 10% edge disorder. However, further increasing vacancy concentration to 20%, we found the edge spins are mostly suppressed, in agreement with previous results [19,20]. Overall, our proposed spin semiconductor is rather robust against a good degree of edge disorder.

In summary, we demonstrate a new spin structure in a ST GNR, the spin semiconductor whose charge carriers are spin polarized not only in energy but also in real space. The spatially separated spin carriers at different edges, which also show a high degree of tunability by electric field and robustness against edge disorder, can be very useful for potential spintronics applications.

This work was supported by ARL (Cooperative Agreement No. W911NF-12-2-0023) and NSF MRSEC (Grant No. DMR-1121252) DOE-BES (Grant No. DE-FG02-04ER46148). S. J. thanks the State Scholarship Fund by the China Scholarship Council for financially supporting her visit at the University of Utah. We thank the CHPC at the University of Utah and NERSC for providing the computing resources.

*Corresponding author.
fliu@eng.utah.edu

[1] M. I. Katsnelson, V. Yu. Irkhin, L. Chioncel, A. I. Lichtenstein, and R. A. de Groot, Rev. Mod. Phys. **80**, 315 (2008).
[2] Y. Son, M. L. Cohen, and S. G. Louie, Nature (London) **444**, 347 (2006).
[3] X. L. Wang, Phys. Rev. Lett. **100**, 156404 (2008).
[4] Y. Li, Z. Zhou, P. Shen, and Z. Chen, ACS Nano **3**, 1952 (2009).
[5] Y. F. Pan and Z. Q. Yang, Phys. Rev. B **82**, 195308 (2010).
[6] X. Hu, W. Zhang, L. Sun, and A. V. Krasheninnikov, Phys. Rev. B **86**, 195418 (2012).
[7] S. Skaftouros, K. Özdoğan, E. Şaşioğlu, and I. Galanakis, Appl. Phys. Lett. **102**, 022402 (2013).
[8] D. Yu, E. M. Lupton, H. J. Gao, C. Zhang, and F. Liu, Nano Res. **1**, 497 (2008).
[9] J. P. Perdew, K. Burke, and M. Ernzerhof, Phys. Rev. Lett. **77**, 3865 (1996).
[10] G. Kresse and J. Hafner, Phys. Rev. B **47**, 558 (1993).
[11] W. Liu, Z. F. Wang, Q. W. Shi, J. Yang, and F. Liu, Phys. Rev. B **80**, 233405 (2009).
[12] D. Yu, E. M. Lupton, M. Liu, W. Liu, and F. Liu, Nano Res. **1**, 56 (2008).
[13] E. H. Lieb, Phys. Rev. Lett. **62**, 1201 (1989).
[14] Z. Liu, J. Wu, W. Duan, M. G. Lagally, and F. Liu, Phys. Rev. Lett. **105**, 016802 (2010).
[15] J. Guo, D. Gunlycke, and C. T. White, Appl. Phys. Lett. **92**, 163109 (2008).
[16] Z. F. Wang and F. Liu, Appl. Phys. Lett. **99**, 042110 (2011).
[17] Z. F. Wang and F. Liu, Nanoscale **3**, 4201 (2011).
[18] Z. F. Wang and F. Liu, ACS Nano **4**, 2459 (2010).
[19] B. Huang, F. Liu, J. Wu, B.-L. Gu, and W. Duan, Phys. Rev. B **77**, 153411 (2008).
[20] J. Kunstmann, C. Özdoğan, A. Quandt, and H. Fehske, Phys. Rev. B **83**, 045414 (2011).